Development of ceramic membranes for resource recovery from brine through percrystallization

Nielsen, Morten Haugaard; Quist-Jensen, Cejna Anna; Ali, Aamer

Published in:
Resources, Conservation and Recycling

DOI (link to publication from Publisher):
10.1016/j.resconrec.2022.106768

Publication date:
2023

Document Version
Publisher's PDF, also known as Version of record

Resources, Conservation & Recycling 189 (2023) 106768

Contents lists available at ScienceDirect

Resources, Conservation & Recycling

journal homepage: www.elsevier.com/locate/resconrec

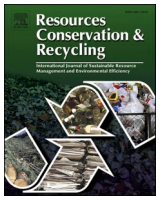

Full length article

Development of ceramic membranes for resource recovery from brine through percrystallization

Morten Haugaard Nielsen, Cejna Quist-Jensen, Aamer Ali *

Department of Chemistry and Bioscience, Aalborg University, Fredrik Bajers Vej 7H, Aalborg, 9220, Denmark

ARTICLE INFO

Keywords:
Percrystallization
Resource recycling
Zero liquid discharge
Membrane synthesis
Ceramic membranes

ABSTRACT

Availability of efficient methods to fractionate a solution into its solid and liquid components is the key to recycling and reuse of industrial effluents. Percrystallization is a novel membrane process where a thin film of warm permeate present at the membrane surface is evaporated through vacuum to crystalize the soluble compounds. Thus, the process separates a solution into crystalline solute and solvent in a single-step and can partly be operated with sustainable sources of energy such as solar and geothermal heat. Since the process is at early stage of exploration, there is no sufficient knowledge about the suitable membrane features for the percrystallization which hampers its further development and potential progress towards commercialization. This work performs a systematic and groundbreaking investigation to identify and develop suitable membranes for percrystallization applications. The study has been carried out by using silicon carbide (Si-C) and polymeric membranes with different porosities and thicknesses. The effect of pore size and surface hydrophobicity on the process operation was investigated by coating the surface of Si-C membranes with methylated silica particles of different sizes. Inherent hydrophobicity of the polymeric membranes was also modified to test their suitability for the percrystallization applications. All the membranes were tested for separation of NaCl crystals from solution by using different concentrations (3.5, 10 and 17.5 wt%) of NaCl at operating temperatures of 50 °C, 55 °C and 60 °C. It was observed that the membranes with the rate of permeation comparable with the rate of evaporation under the applied vacuum are crucial to operate the process. Thus, only less porous and thick Si-C membranes with liquid entry pressure approaching to 1 bar were suitable for percrystallization. The developed membranes yielded water and NaCl flux in the range of 9.43±2 and 1.2 kg/m^2·h, respectively. The process outperformed state-of-the-art membrane processes in terms of productivity and simplicity.

1. Introduction

Conventional resources of raw materials and freshwater are under extreme stress due to the rapidly increasing population, improve lifestyle and industrialization (Elshkaki et al., 2018; Ali et al., 2017; Peter, 1993). The scarcity of freshwater is considered among the most critical global challenges of the current era as it threatens sustainable development and the economic growth (Vörösmarty et al., 2010; Mekonnen and Hoekstra, 2016; Schwarzenbach et al., 2010). The quality of many resources of freshwater has significantly degraded due to the release of natural as well as artificial pollutants to the environment (Meybeck, 2003; A. Panagopoulos and Haralambous, 2020). Several environmental regulations have been imposed on industries to limit their contribution to the environmental pollution. To comply with the new regulations, zero liquid discharge (ZLD) technologies have emerged which aim to concentrate waste ideally to the complete dryness (Vergili et al., 2012; Yaqub and Lee, 2019). If possible, water is reclaimed during ZLD treatment so that it can be recycled within the process (Yaqub and Lee, 2019; Tong and Elimelech, 2016; Oren et al., 2010). At the same time, the soluble compounds (minerals or pollutants) are obtained in solid form which makes their management (reuse or disposal) feasible.

State-of-the-art ZLD systems used to treat brine consist of brine-concentrator, crystallizer and -evaporation pond. Although water is reclaimed during concentration and crystallization, these processes are associated with high capital cost, large physical footprint and/or a large consumption of electricity or carbon-based fuels (A. Panagopoulos and Haralambous, 2020; A. Panagopoulos and Haralambous, 2020). Efforts are continuously made to increase the cost efficiency of traditional ZLD systems. Many such novel solutions are membrane-based and are applied either as a pretreatment to decrease the volume of wastewater

* Corresponding author.
E-mail address: aa@bio.aau.dk (A. Ali).

https://doi.org/10.1016/j.resconrec.2022.106768
Received 25 July 2022; Received in revised form 4 November 2022; Accepted 8 November 2022
Available online 17 November 2022

Table 1
Molar ratios of reactants and temperatures used to produce methylated silica nanoparticles. The molarity of water in the reaction is displayed as the moles of distilled water added + the moles of water present in the transferred ammonia solution.

Sample	TEOS $\left[\frac{mol}{L}\right]$	MTES $\left[\frac{mol}{L}\right]$	NH_3 $\left[\frac{mol}{L}\right]$	H_2O $\left[\frac{mol}{L}\right]$	EtOH $\left[\frac{mol}{L}\right]$	Temperature $[^{\circ}C]$
P1	1	0.67	4.33	16.67+2.94	58.00	60
P2	1	0.67	4.22	7.17+2.15	86.50	70
P3	1	0.67	4.29	7.24+2.54	71.29	60
P4	1	0.67	3.33	3.67+1.70	86.50	70

prior to conventional ZLD treatment system or as an alternative to the conventional ZLD system (Yaqub and Lee, 2019; Chabanon et al., 2016). Reverse osmosis is considered the most energy efficient pretreatment to apply before ZLD technologies but it cannot treat high-concentrated solutions (Elimelech and Phillip, 2011; Al-Karaghouli and Kazmerski, 2013; Gude, 2011). Membrane distillation and membrane crystallization are excellent at utilizing waste-grade heat to concentrate solutions. The membrane crystallization process eventually generates a fine slurry of crystals (Chabanon et al., 2016; Drioli et al., 2012) therefore, filtration and drying steps are needed to obtain a dry product which add additional complexities (Chabanon et al., 2016). Moreover, the membrane must comply with the stringent requirements of high resistance to the scale formation and liquid intrusion into the pores.

Membrane percrystallization is emerging as an alternative to the conventional ZLD systems. Percrystallization separates saline solutions to yield distilled water and dry crystals in a single step. The working system consists of a warm feed solution passing through a membrane without any retention of the dissolved components (ions, molecules etc.). The liquid permeating through the membrane is evaporated to precipitate the dissolved solids in form of crystals. The heat required to warm the solution can potentially be supplied through a source of low-grade heat such as solar or geothermal heat. The first papers reporting percrystallization applied polymeric collodion bags while recent papers used inorganic membranes with a carbon coating where a vacuum drives the permeation and evaporation (H. Tauber and Kleiner, 1932; H. Tauber and Kleiner, 1932; Yamamoto et al., 1973; Skov and Madsen, 1968; R.S.K. Madsen et al., 2018; R.S.K. Madsen et al., 2018; Madsen et al., 2019). Availability of suitable membranes is of fundamental importance to ensure the stable performance of the process over long term. For a smooth operation of the percrystallization process, identification of suitable membrane features and operative conditions that ensure continuous detachment of the crystals from the membrane surface is also crucial. Other important aspects of the process, which are not yet well understood include thermal optimization, module design and membrane requirements to crystalize a specific compound.

The recent research in percrystallization process is mainly revived by the research group of Joao da Costa who applied sugar-coated inorganic membranes to conduct the percrystallization process (R.S.K. Madsen et al., 2018; Madsen et al., 2019; Motuzas et al., 2018). The group reported crystallization of different salts, food ingredients and pharmaceutical compounds through percrystallization. The authors identified the membrane material and pore diameter as the key membrane features for a successful operation of percrystallization process (R.S.K. Madsen et al., 2018). Thus, the authors reported that the percrystallization could be achieved through mesoporous ($3 \leq dp \leq 9$ nm) titania, gamma-alumina and carbon membranes, but not with other membrane materials such as sub-nano (dp <0.5 nm or 5 Å) silica, carbon molecular sieves, nor microporous α-alumina substrates (dp~150 nm). In a more recent study carried out by Ji et al., a membrane consisting of α-Al_2O_3 substrate, γ-Al_2O_3 interlayer, and SiO_2 top layer, where the average pore size of the top layer was ~1.5 to 5.7 nm, was successfully applied to carry out the percrystallization process (Ji et al., 2022). Like the aforementioned studies, the successful operation of the process was attributed to the mesoporous structure of the material. Although, these studies demonstrated potential of the process for crystallization of different compounds, yet the currents state-of-the-art does not provide clear guidelines about the suitable membrane features for the percrystallization process.

The current study aims at extending the understanding of suitable membranes for percrystallization by exploring the effect of hydrophobicity, overall porosity, pore size and thickness of the membrane on operation of the percrystallization. Our hypothesis is that the rates of permeation and evaporation dictate the operation of the percrystallization process; and since the permeation is not controlled only by the membrane pore size and material—the only two parameters reported in the previous studies on percrystallization (Motuzas et al., 2018), (Ji et al., 2022)—therefore, other permeation-controlling parameters (hydrophobicity, overall porosity, and thickness) are also worth investigating. The study is carried out by modifying and testing commercial ceramic and polymeric membranes for percrystallization applications. This is accomplished by functionalizing silicon carbide (Si-C) microfiltration membranes with methylated silica particles to modify the pore size and surface hydrophobicity which control the permeability. A relatively more porous and thinner polymeric membrane has been used to investigate the effect of overall porosity and thickness—two other permeation-controlling parameters—on the process performance. The goal is to ultimately identify the suitable membrane features for percrystallization process to make it a technically viable ZLD candidate.

2. Materials and methods

2.1. Materials

Si-C microfiltration membranes, with an average pore size of 3 μm, were provided by LiqTech. The membranes are cut into ~10 cm long pieces before further treatment.

Tetraethyl orthosilicate (TEOS) (98%), Triethoxymethylsilane (MTES) (99%) and trichloro(octyl)silane (97%) were purchased from Sigma-Aldrich. Ammonium hydroxide (25%) was purchased from Honeywell Fluka, absolute ethanol (EtOH) (99.8%) and n-Hexane (97%) were purchased from VWR Chemicals. Sodium chloride (NaCl) (>99%) was purchased from Chemsolute—Th. Geyer.

2.2. Synthesis of methylated silica particles

The methylated silica particles were prepared as colloidal silica sols via modified Stöber method (Yang et al., 2010; Li et al., 2020; Purcar et al., 2014). The molar ratios of the reactants used for synthesis are provided in Table 1. Demineralized water and ammonia were added to 1/3 the volume of EtOH. In a separate beaker, TEOS was added to 1/3 the volume of EtOH. The mixtures were combined and heated to 60 °C or 70 °C (see Table 1) where it was left to react for 90 min. In a separate beaker MTES was added to 1/3 the volume of EtOH and this solution was added to the reaction mixture. The mixture was heated at 60 °C for 19 h. Lastly, the solution was set to age while stirring at ambient conditions for 3 days.

Silica networks were formed according to the typical hydrolysis (reaction 1) and condensation (reaction 2) reactions of alkoxy silanes.

$$2\ Si{-}OR + 2\ H_2O \rightarrow 2\ Si{-}OH + 2\ ROH \quad (1)$$

$$2\ Si{-}OH \rightarrow Si{-}O{-}Si + H_2O \quad (2)$$

Ammonia was used as a catalyst where monodisperse silica particles were formed via the initial hydrolysis and condensation of TEOS according to the original Stöber method (Stober et al., 1968). Later in the process, organo alkoxy silane, MTES, was added where the silica particles grew further and attained hydrophobic properties according to the well-established modified Stöber method (Yang et al., 2010; Li et al., 2020; Beganskienė et al., 2004; Tadanaga et al., 2013).

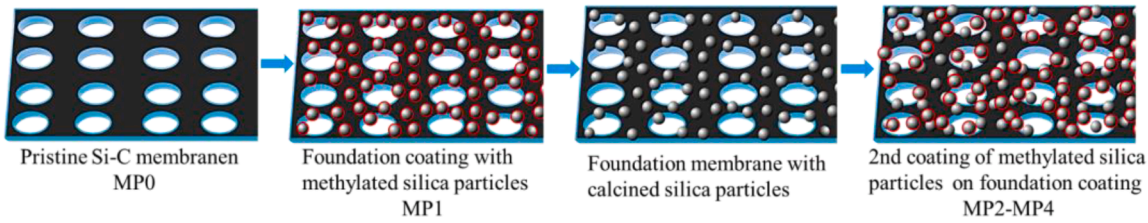

Fig. 1. A schematic diagram of the Si-C membrane modification via foundation particle coating, calcination and surface particle coating. Silica particles and methylated silica particles are illustrated with simple spheres and spheres with the circle around, respectively.

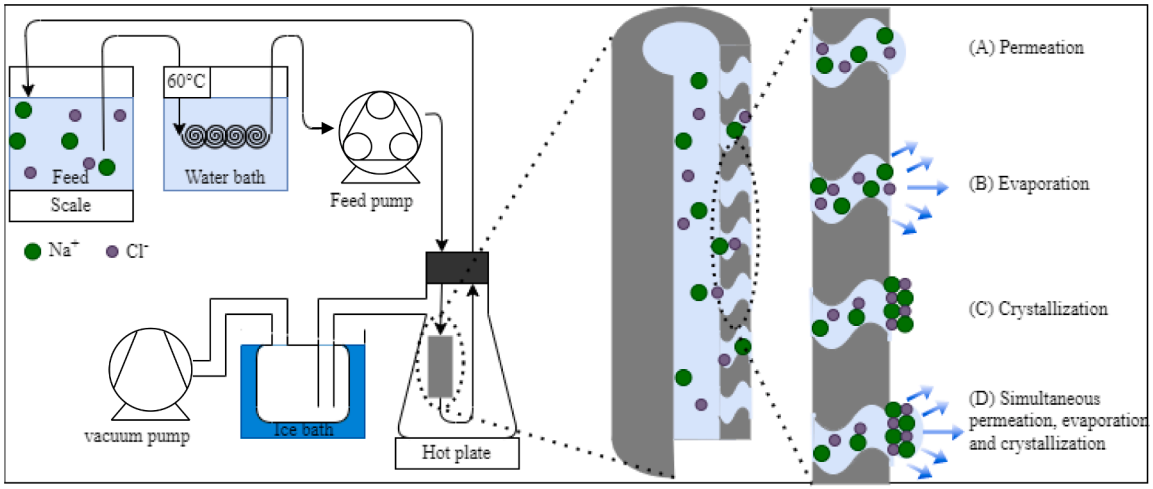

Fig. 2. Schematic diagram of the percrystallization setup used in this work and an illustration breaking down the different phenomena occurring during the percrystallization process.

Approximately 10 min. after adding TEOS to the reaction, a turbid white mixture was obtained which was the first indication of the formation of colloidal silica sol. This phenomenon is attributed to the light scattering properties of submicron silica particles (Gao et al., 2016).

2.3. Characterization of methylated silica nanoparticles

2.3.1. Particle size analysis

The hydrodynamic diameter of the methylated silica particles in the sol was analyzed by dynamic light scattering (DLS) using a Malvern Zetasizer Nano - ZS. The particles were analyzed over a concentration range obtained by diluting the methylated silica sol with absolute EtOH.

2.4. Coating of Si-C membranes

Membrane segments were immersed sequentially in EtOH, acetone and demineralized water (10 min in each) before drying at 100 °C for 12 h. Afterwards, membrane segments were immersed in silica sol for 5 min followed by drying at 100 °C for 30 min. The coating process was repeated for 5 times. All the membranes were first coated with a base coating of the largest synthesized particles to provide a foundation for smaller particles. Afterwards, 3 out of 4 membranes were calcined at 500 °C for 10 h, where all organic matter was thermally degraded, yielding a pure silica coating ready for a second coating with different sized methylated particles synthesized according to the Table 1. The last membrane was annealed at 400 °C for 2 h yielding a membrane with a hydrophobic coating of the largest particle size. A schematic diagram of the steps involved in the membrane modification process can be seen in Fig. 1.

2.4.1. Characterization of Si-C membranes

(i) X-ray diffraction analysis

A pulverized sample of the pristine membrane was analyzed by X-ray diffraction (XRD) at 2θ ranging from 10°to 90°using a Panalytical Empyrean diffractometer with a Cu-K-α radiation source ($\lambda = 1.5419$ Å) with a Ni-filter.

(i) *X-ray photoelectron spectroscopy*

X-ray photoelectron spectroscopy (XPS) was used to characterize the surface elemental compositions. Membrane samples were cut into pieces of 1 × 1 cm. The x-ray source was Specs XR50 and detector was Specs Phoibos 150. X-ray emission energy with Al of 1486 eV was used. The XPS survey spectra was performed in appropriate spectrum ranges for C1s and Si2p with step-size of 0.1 eV and pass energy of 30 eV.

(i) *Water contact angle analysis*

Water contact angle (WCA) was determined by optical tensiometry using Biolin Scientific Attension Theta Lite in sessile drop mode. The analysis mode of the apparatus was "Contact angle (Young-Laplace)". 10 μL droplets were dispensed at a rate of 1 $\mu L/s$ and were manually placed on the surface of the membrane and the images were recorded over a duration of 5 min.

(i) *Porosity determination*

The total volume of membrane samples was determined via the Archimedes principle (Hughes and Lau, 2008) by submerging samples in a 10 vol% EtOH solution with a density of 0.9865 g/mL. Membranes

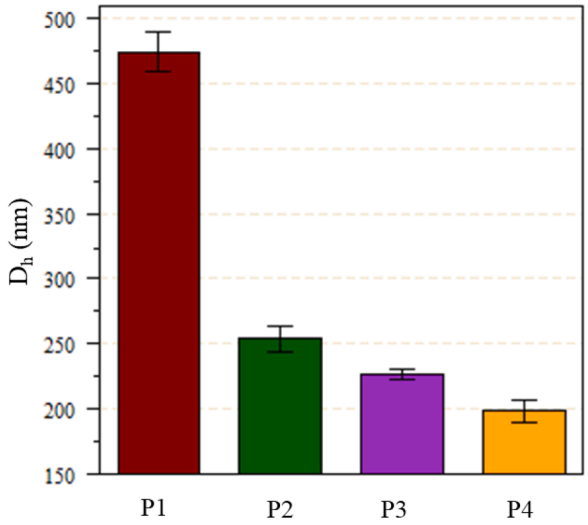

Fig. 3. Hydrodynamic diameter of methylated silica particles synthesized according to the conditions provided Table 1.

were coated in a 5 vol% trichloro(octyl) silane in n-hexane solution for 30 min to stop the liquid penetration into the membrane pores (Giang et al., 2020).

The volume of dense membrane material, i.e. non-porous volume of the membrane, was determined by He-pycnometer (Ultrapyc 1200e, Quan-tachrome). This measure was used in conjunction with the total volume to determine the void volume (porosity) of the membranes.

(i) *Scanning electron microscopy*

The surface morphology of the membrane was studied by using scanning electron microscopy (SEM). Membrane samples were coated with a layer of gold by an Edwards Sputter Coater S150B prior to SEM imaging through a ZEISS GEMENI 1540 XB using 10 kV acceleration voltage.

(i) *Atomic force microscopy*

The surface roughness of the membranes was analyzed with atomic force microscopy (AFM) with a scanning area of 20 × 20 μm. The derived AFM images were analyzed by Gwyddion 2.61.

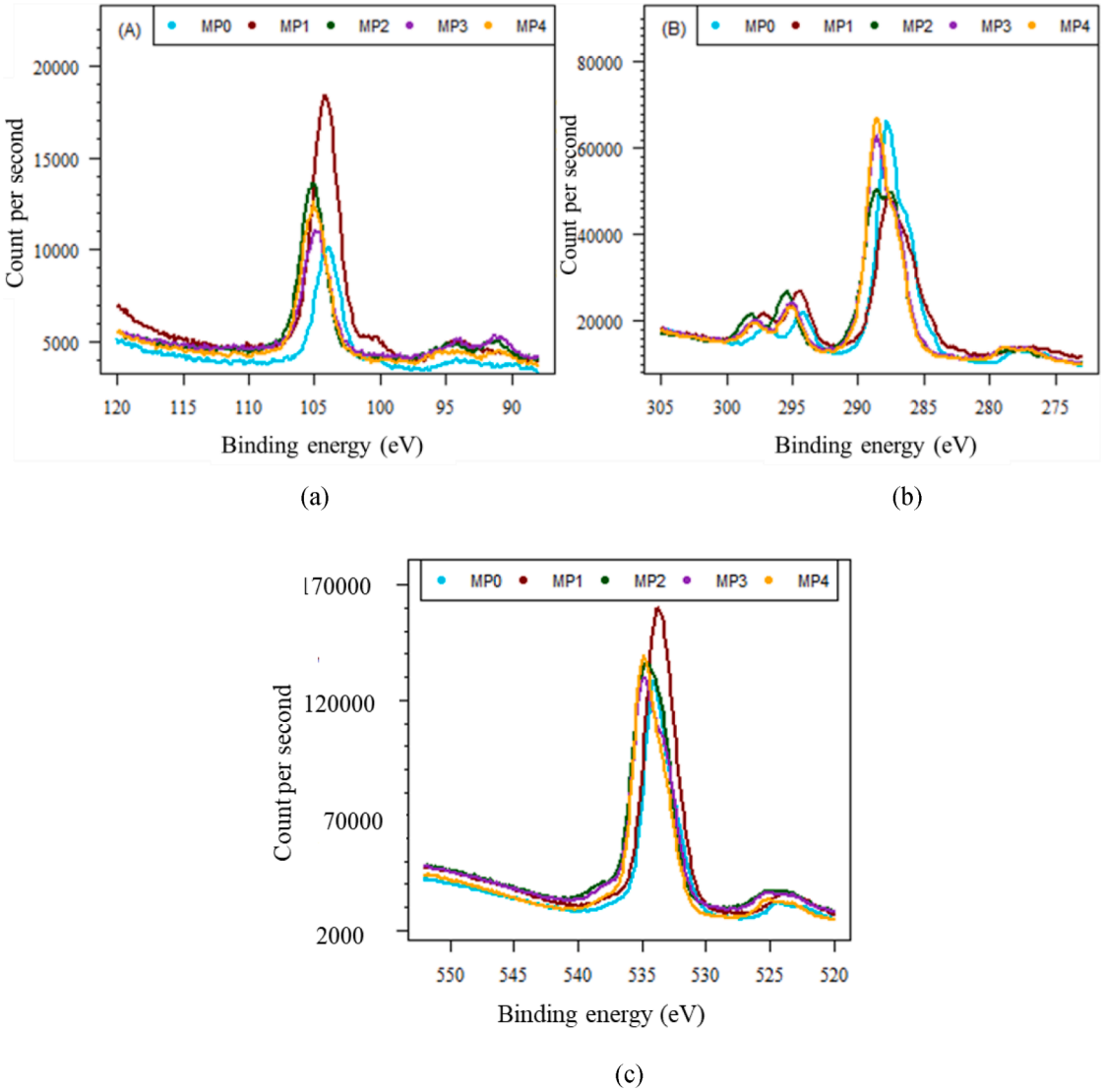

Fig. 4. XPS spectra for (a), Si2p (b) C1s and (c) O1.

Table 2
Surface composition and C/Si ratio of the different membranes.

	O	C	Si	C/Si ratio
MP0	61.7	34.5	3.9	8.9
MP1	67.8	22.7	9.5	2.4
MP2	64.2	29.6	6.2	4.8
MP3	63.2	31.6	5.2	6.1
MP4	63.5	33.2	3.4	9.8

2.5. Polymeric membrane

Polypropylene (PP) Accurel s6/2 (Membrana, GmbH) hollow fiber membrane was used. The membrane had overall porosity of 73%, wall thickness of 450 μm, average pore size of 0.2 μm and liquid entry pressure greater than 1.4 bar (Drioli et al., 2013). Due to the hydrophobic nature of this membrane, wetting had to be induced to allow the water permeation. To control the rate of permeation through the membrane pores, isopropanol alcohol (IPA) and Triton x-100™ in concentration ranges of 0.5 – 8 wt% and 50 – 500 ppm, respectively were pushed through the membrane pores.

2.6. Percrystallization tests

The experimental setup to perform percrystallization is inspired by the setup used by Juan et al. and it is illustrated in Fig. 2 (Moltedo et al., 2022). A picture of the lab-scale setup is provided in the Appendix (Fig. A1). The membrane was housed in a flask where the vacuum was created with a vacuum pump. The flask was heated by a hotplate set at 50 °C to prevent the accumulation of vapor inside the flask. The feed was pumped into the membrane after heating in a water bath. A vacuum pressure of 200 mbar was created on shell side of the membrane to pull the liquid through the membrane pores. The liquid film from the membrane surface evaporated under the combined effect of applied vacuum and temperature of the feed solution. The vapor was condensed in the cold trap to recover the freshwater. Solutions of 3.5, 10 and 17.5 wt% NaCl in demineralized water were used for percrystallization where each solution was tested at 50 °C, 55 °C and 60 °C.

3. Results and discussion

3.1. Particle size analysis

The hydrodynamic diameter (D_h) of the synthesized particles is shown in Fig. 3. It is evident from Fig. 3 that the average particle size varies from 198 to 475 nm, depending upon the synthesis conditions applied. The size of the particles synthesized through the Stöber method varies greatly according to the temperature and composition of the reaction mixture due to different degree of nucleation and growth rate (Bhattacharjee, 2016).

Matsoukas et al. studied the Stöber method and determined that initially the rate of nucleation is the dominant process, but it eventually decays to insignificant levels and growth becomes the dominant process (Matsoukas and Gulari, 1988). The kinetics of these processes are determined by the reaction temperature, NH_3 concentration and H_2O concentration where increase in H_2O and NH_3 concentrations positively influence the particle size. Increase in reaction temperature decreases the particle size as shown in the literature (Bhattacharjee, 2016). In practice, increasing NH_3 concentration increases the particle size which holds true for all but the P3 sample. The size of P3 is smaller than P2 even though it has higher NH_3 and H_2O concentrations compared to P2. Possibly, the effect of high reaction temperature for P3 overcomes the combined effect of high NH_3 and H_2O concentration, which tends to increase the particle size, and therefore the average particle size decreases (Park et al., 2002). Thus, the discrepancy in size for P3 can be explained by the increase in H_2O concentration. These trends are also observed in the literature where the Stöber method is proven highly customizable and various combinations of reactant concentrations and temperatures produce particles of various size (Tadanaga et al., 2013; Ghimire and Jaroniec, 2021).

3.2. XPS analysis

XPS measurements for Si2p, C1s and 1O are presented in Fig. 4(a) and (b) and c), respectively, to identify the Si-, C- and O-binding. The peaks for Si2p (Fig. 4a) around binding energy of 103.5 eV account for SiO_2. The peaks for the coated membranes are higher than for the pristine membrane since the membranes are coated with silica particles. The peak intensity decreases for MP1 to MP3 due to smaller particle sizes in the coating. However, for MP4 the peak increased compared to MP3, which is also similar for C1s and O1s. The peaks in Fig. 4(b) are related to Si-C, C—C and C—O binding (~284–287 eV), which increases and moves slightly to higher binding energies with decrease in the size of coating particles. This indicates that the coating gets more uniform with decrease in particle size. The main peak in Fig. 4(c) can account for SiO_2 (532.9 eV) and residue H_2O (~534 eV). The surface composition of the membranes is shown in Table 2. It is observed that the C/Si ratio is high for the pristine Si-C membrane, then decreases for MP1 and the increases again with decrease in particle coating.

3.3. SEM imaging

The recorded SEM micrographs are illustrated in Fig. 5. The surface of MP0 consists of regions composed of large grains and porous areas connecting these grains. The pores are unequal in size ranging from several microns to submicron. Moving from MP1 to MP4, the particles observed in the micrographs clearly decrease in size, which agrees well with the results obtained through DLS measurements. MP1 is the membrane with the largest particle coating as also clearly visible in the corresponding SEM image. As a result of the coating, the grains and porous areas become less distinct, and the membrane surface becomes more homogeneous. It is also evident from the figure that MP1 and MP2 have some macrovoids in their structure and the surface is relatively more homogeneous for MP3 and MP4.

On the other hand, MP3 and MP4 samples exhibit cracks on their surfaces which are not present in the pristine material. Relatively smaller (~0.3 μm) cracks-widths are present at the surface of MP3 and their size increases in MP4. Similar findings are reported by Huertas et al. who coated sol-gel particles onto LiqTech Si-C membranes (Huertas et al., 2017). The cracks are identified as microcracks and are believed to stem from sub-optimal sol-gel particle coating or very high heating rate (A. Alem et al., 2009; A. Alem et al., 2009). The coatings with small particles are more susceptible to microcracks as also observed in the current study where microcracks became more significant for the small particle sizes.

3.4. AFM analysis

The observation made through SEM images are confirmed by AFM images (Fig. 6), where the surface of MP0 contains few large and broad peaks. The coating of MP1 and MP2 results into the formation of larger peaks on their surface compared to MP3 and MP4 and some macrovoids are visible in the dark areas. The surface topography is different for MP3 and MP4, where the peak size reduces but the number of peaks increases as eventually the peaks start merging for MP4 providing it more smoothness than MP3. This also confirmed by analysis of the average surface roughness (Ra) and root mean square roughness (R_q) (Table 3), which decreases for MP3 and MP4. The same tendency is observed in the SEM images (Fig. 5), where the surface does not show any macrovoids for MP3 and MP4.

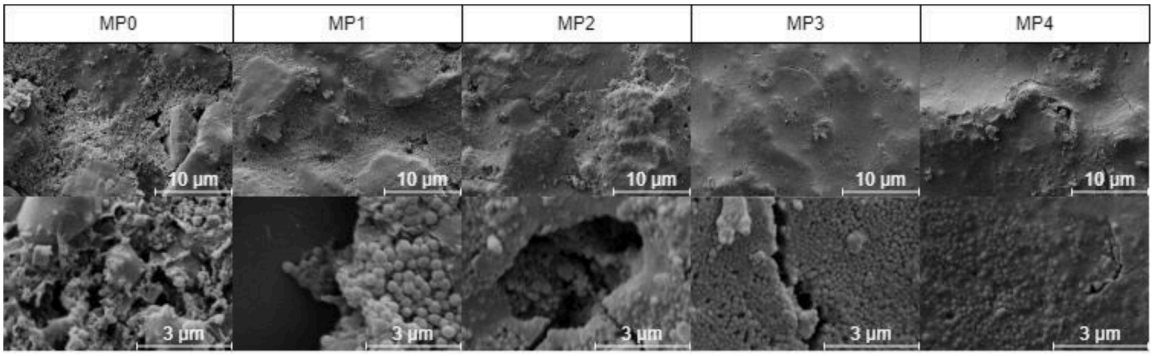

Fig. 5. SEM images of the membrane surfaces. Upper frames are at ~1220 X magnification and the lower ones are at ~15,520 X magnification.

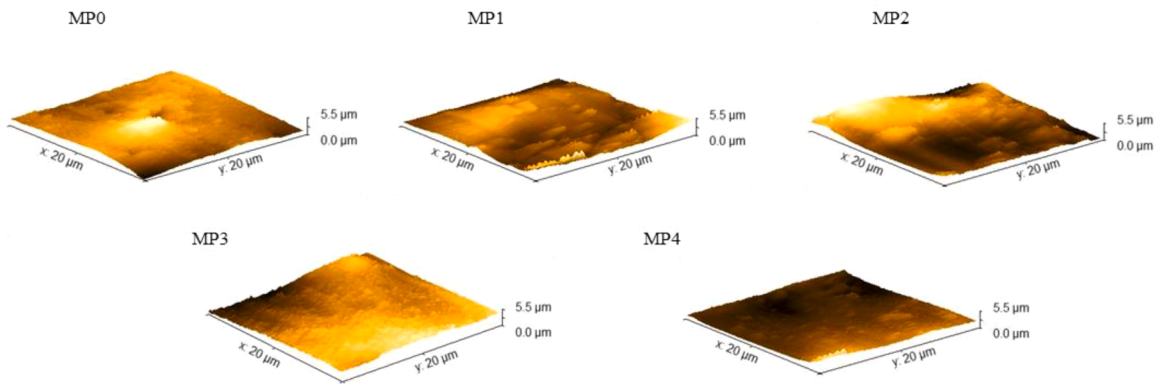

Fig. 6. AFM images of the membrane surfaces.

Table 3
Surface roughness of the different membranes.

	Average surface roughness (R_a) [nm]	Root mean square roughness (R_q) [nm]
MP0	30.49	36.13
MP1	63.98	76.55
MP2	90.31	103.1
MP3	78.52	101.8
MP4	57.63	66.18

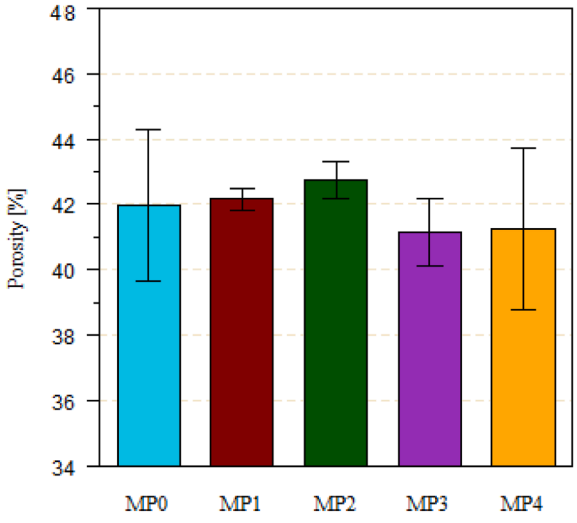

Fig. 7. Porosity of the pristine and modified membranes.

3.5. Porosity

The porosity of the pristine and modified membranes is determined by using the volumes obtained by Archimedes principle and He-pycnometry. The porosity is calculated according to Eq. (3) and the results are displayed in Fig. 7.

$$\frac{V_{void}}{V_{total}} = \frac{V_{Archimedes} - V_{Pycnometry}}{V_{Archimedes}} \tag{3}$$

The porosity of the series of membranes ranges from 41% to 43%. It appears that the coating does not affect the overall porosity of the modified membranes which is an indication that the particles were present only at the membrane surface. If the coating were also penetrated inside the membrane pores, then the porosity would logically decrease as membrane pores would be filled, to some extent, with the particles. However, this is not clearly observed as the error bars of the values have a significant overlap which indicates that the particles are present only at the surface of the membrane and the bulk is still porous.

3.6. Water contact angle analysis

WCA at the membrane surfaces was measured (see Fig. 8) to analyze the effect of the modifications on surface hydrophobicity of the membranes. Pictures of the water droplets on the membrane surfaces can be seen in Fig. A4 in the appendix in the range of 0 to 5 min. Inspecting the WCA plots from left to right in Fig. 8, it appears that the pristine membrane (MP0) has relatively lower WCA and the steepest downward slope over the duration of the measurements due to the hydrophilic nature of the pristine Si-C (Ma et al., 2019). The membrane surfaces coated with methylated silica particles (MP1 through MP4) have high WCA due to their hydrophobic properties as also observed in the literature (Yang et al., 2010).

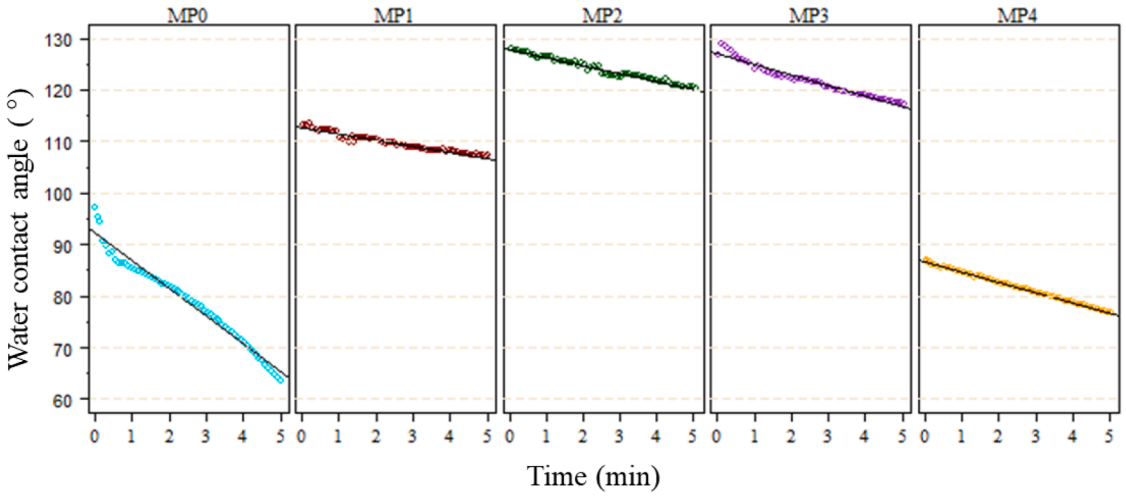

Fig. 8. Water contact angle measurements from 0 to 5 min of the membranes MP0 to MP4.

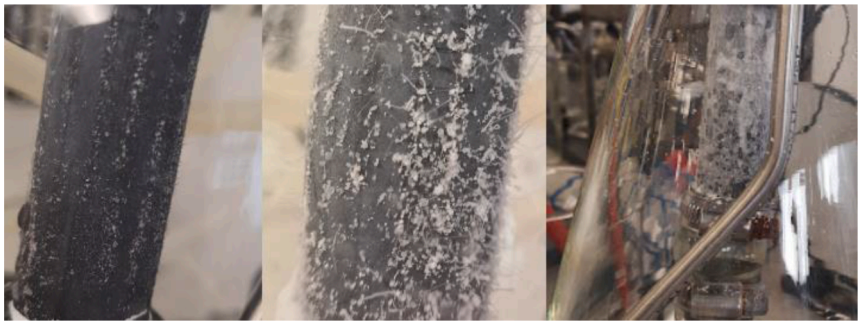

Fig. 9. (a) The surface of MP3 after a few minutes of percrystallization where initial NaCl crystals are clearly visible. (b) needle shaped NaCl crystals clearly visible after ~ 20 min of percrystallization (c) the crystals obtained after running the experiment multiple times.

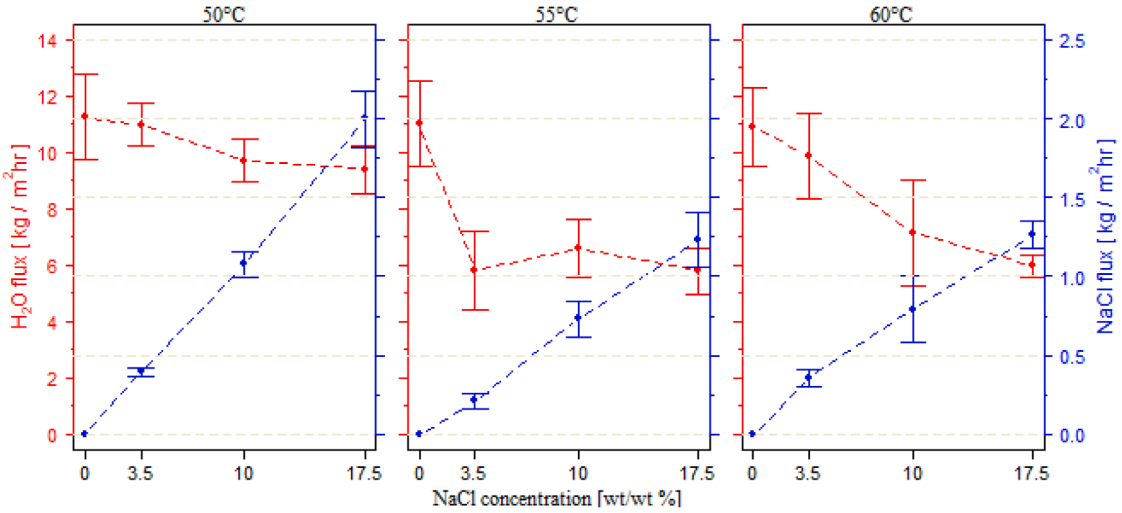

Fig. 10. Salt and water flux at different concentrations and temperatures applied in the tests.

MP1 is coated with the largest particles and exhibits higher WCA than MP0. This tendency continues for MP2 and MP3 which demonstrate WCA even higher than MP1. This indicates that the second coating of these samples is successful in further improving the hydrophobic properties of the membranes. This tendency is observed elsewhere and described how the design of surface roughness affect contact angle (Wolansky and Marmur, 1999). In simple terms, hierarchical rough surfaces (see Section 3.4) appear more hydrophobic than plain surfaces or simple rough surfaces (Cortese et al., 2008).

The tendency of increase in WCA with decreasing particle size does not hold true for MP4. The slope of WCA of MP4 is not as steep as that of MP0 which indicates some change in membrane properties when compared to MP0; nevertheless, the observed WCA remains lower than the other modified membranes. Reasons for the observed lower WCA of

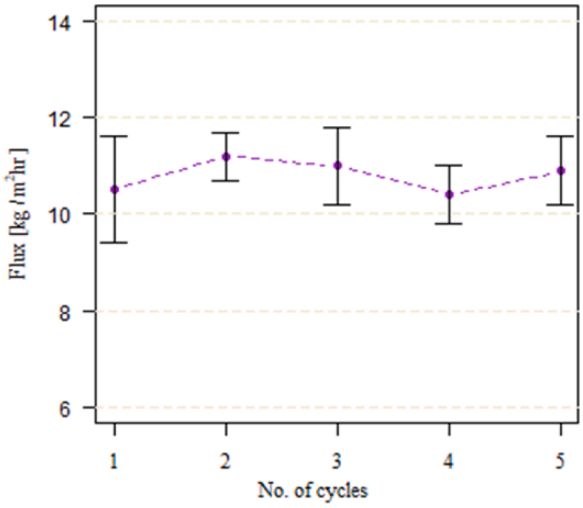

Fig. 11. Water flux as function of number of testing cycles.

MP4 are the relatively smaller size of the methylated silica particle used in the modification and better surface coverage which gives it smoothness. This is consistent with the measured surface roughness (Table 3), which is lower for MP4 compared to MP1-MP3. It is also reported in the literature that the surface roughness smaller than a threshold size and surface coverage exceeding than a certain level is not effective in enhancing the WCA (Zhang, 2021). This is also observed through the AFM images (Section 3.4), where it is noticed that the height of the peaks reduces from MP1 to MP4, but the number of peaks and therefore, the surface coverage increases which is possibly another factor contributing to the observed low WCA as indicated in the literature (Zhang, 2021).

3.7. Initial percrystallization experiments

Percrystallization is initially carried out with all the membranes with 17.5 wt% NaCl solution at 60 °C. These conditions are selected to maximize the rate of evaporation and to ensure that only a small amount of liquid needs to be evaporated before crystals start forming.

3.7.1. Polymeric membrane

Due to its high liquid entry pressure (1.4 bar), the initial percrystallization tests on pristine PP membrane were tried at high transmembrane pressure where the applied vacuum pressure was combined with external hydraulic pressure. However, the control over rate of permeation was not possible. When the total transmembrane pressure was less than the liquid entry pressure of the membrane, indeed no permeation was observed. As soon as the applied pressure exceeded the liquid entry pressure, a very flux (>70 kg/m^2.h) was observed. The combination of applied vacuum and feed temperature was not sufficient to instantaneously evaporate the permeate which starts trickling down from the fiber. The observed high flux was expected as PP membrane is highly porous and has only small thickness which ensures that the liquid permeation faces very low resistance when the applied pressure is above the liquid entry pressure. This resulted into high flux and therefore, flooding of the fiber.

In the next step, the efforts were devoted to lower the resistance to the liquid intrusion of the PP membrane by pushing different compositions of isopropanol alcohol (IPA) and Triton x-100™ through the membrane pores followed by washing the pores with pure water before introducing NaCl solution. The treatment was indeed useful in reducing the liquid entry pressure of the membrane, however, the permeate flooding was observed in all the cases and a continuous percrystallization could not be achieved. Therefore, it was concluded that highly porous and thin PP membranes were not suitable for the percrystallization applications.

3.7.2. Ceramic membranes

The pristine ceramic membrane, MP0, had too high permeability (>90 kg/m^2.h under the applied vacuum) which, like PP membrane,

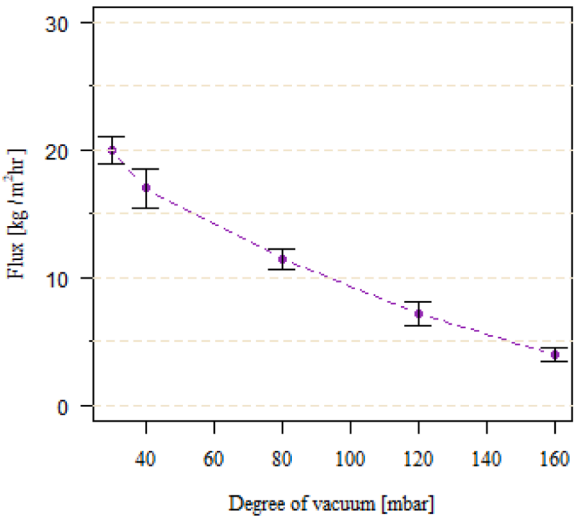

Fig. 13. Effect of applied degree of vacuum on water flux of MP3 membrane operating at 50°C.

(a) Shell formation (b) Flake ejection (c) Powder ejection

Fig. 12. Modes of NaCl crystal formation observed during percrystallization with MP3. (a) a stable crystal shells may form (b) A thin shell is formed around the membrane, but the liquid-vapor transition is sufficient to break chunks of crystal off the membrane. (c) crystal powder is continuously ejected from the surface after initial accumulation at the surface.

Fig. A1. A picture of the percrystallization set up used in the study for testing Si-C membranes.

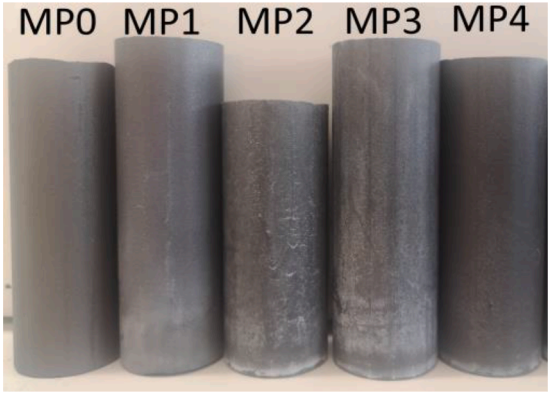

Fig. A2. Picture of the membranes used in the current study.

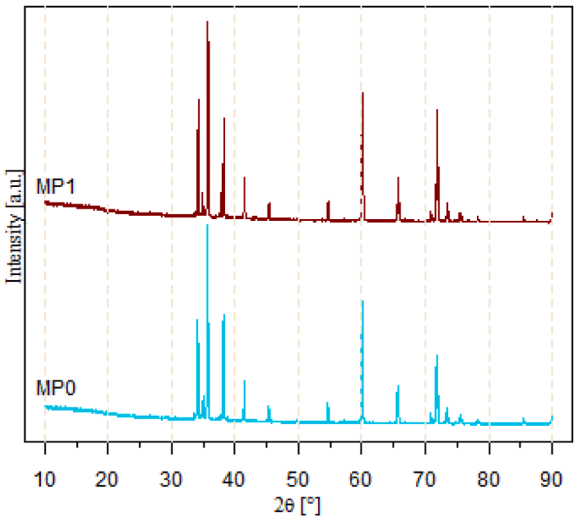

Fig. A3. X-ray diffractogram of MP0 and MP1 measured from 0°to 90°

caused the membrane flooding. This is expected due to the hydrophilic character of this membrane and the presence of macropores in its structure. These hydrophilic microfiltration membranes are primarily designed to retain colloids and suspended particles while maximizing permeation of the liquid. Once the vacuum is applied, a large volume of liquid permeates through the membrane which causes the membrane flooding. These observations highlight the need to modify these membranes to make them suitable for percrystallization. The same observations are valid for the membranes MP1, MP2 and MP4 with the exception that wetting occurs at a slightly higher degree of vacuum (0.2–0.4 bar) compared to MP0. MP3, however, behaved differently and showed no permeation up to 2 bar transmembrane pressure (TMP). According to Franken et al., liquid entry pressure is a function of the pore geometry factor (B), liquid surface tension (γ_l), liquid contact angle (θ) and the maximum pore size (Eq. (4)) (Franklin et al., 1987).

$$\Delta P = P_F - P_P = -\frac{2 * B * \gamma_l * \cos(\theta_l)}{r_{max}} \tag{4}$$

MP2 and MP3 share approximately the same WCA which suggests that the observed change in LEP is determined by changes in the maximum pore size. As evident from Fig. 5, the surface of MP3 contains very small (<0.1 μm) pores and some cracks with thickness less than 0.3 um. Thus, small pore sizes combined with high WCA results into high LEP for MP3. MP2, on the other hand, has many macrovoids at the surface which, despite its high contact angle, drastically reduced its resistance to the water penetration.

No liquid readily permeated the MP3 membrane therefore, the saline feed was replaced with 96% (v/v) EtOH solution to wet the pores of the membrane. This is possible as EtOH has a lower surface tension compared to water which allows it to intrude into the pores more easily (Eq. (4)). Hereby complete wetting of the MP3 membrane was obtained at 2 bar TMP and consistent permeation was observed in a shorter time span.

Afterwards, EtOH solution was replaced with distilled water to wash the pores of the membrane, while keeping the membrane wetted for 2 h at 1 bar TMP. Afterwards, the saline solution was retried and at this point, a very controlled rate of solution permeation was observed under the applied vacuum and crystals readily appeared on surface of the membrane. Thus, the ethanol infiltration facilitated the water transport through the pores under the applied vacuum.

As the process went on, needle-like crystals started growing perpendicular to the membrane surface, as can be seen in Fig. 9(b), which contrasts with the fine NaCl particles Madsen et al. obtained by percrystallization with a ceramic membrane [(R.S.K. Madsen et al., 2018). These needle-like crystals resemble with those obtained by collodion bag percrystallization (H. Tauber and Kleiner, 1932), silica gel percrystallization (Hinegardnrr, 2022) and seem to be a close match to the needle-like salt whiskers Ji et al. recently documented by performing percrystallization on an organic/inorganic hybrid membrane with a silica-rich inorganic surface (Ji et al., 2022). Ji et al. also analyzed the growth mechanism of the formation of needle shaped crystals and found that cubic segments crystallize on the surface of the membrane. These cubic segments form a foundation for further growth of the salt crystal (Ji et al., 2022). From the foundation, the needles continue to grow due to the creeping of saturated salt solution. Saturated solution essentially covers the salt crystal and ions deposit onto the existing surface as liquid evaporates. At the tip of the needle, the curvature of the liquid accelerates the rate of evaporation of the liquid, according to the Kelvin equation (Al-Kindi and Babadagli, 2021), which promotes the growth of crystals perpendicular to the membrane surface resulting into the formation of needle-like crystals (van Enckevort and Los, 2013).

After ending the initial experimental campaign and washing the surface of the membrane, the process was repeated. While percrystallization occurred, no needle-like crystals grew from the membrane surface. Either the membrane surface had been disturbed in such a way that

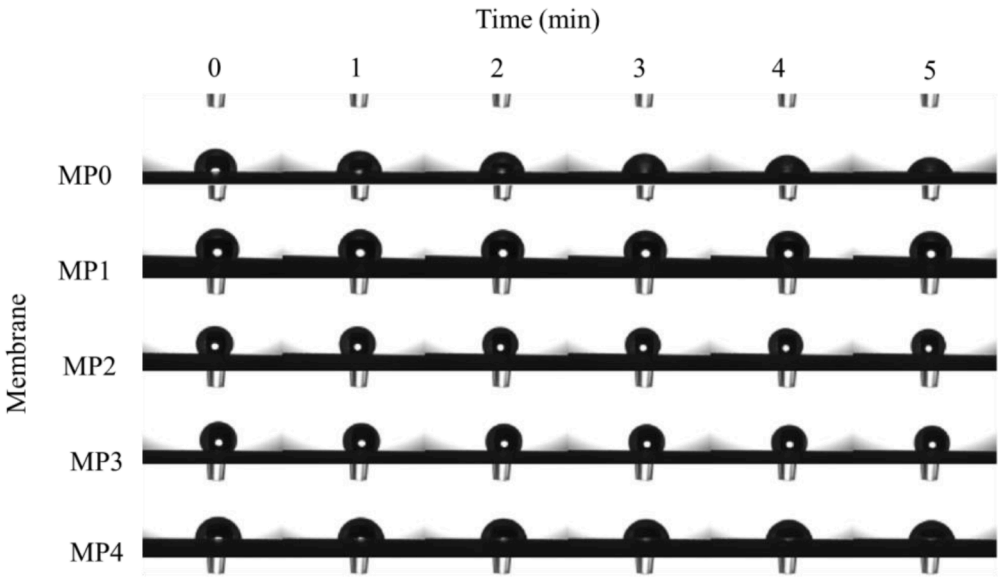

Fig. A4. The pictures of water droplet on surface of different membranes at different times.

the conditions for needle-like growth were not met, or crystals covered the surface of the membrane which suppressed the formation of the needle-like crystals. Regardless, further studies are needed to investigate the membrane features and operating variables which induce the formation of needle-like crystals.

3.8. *Effect of temperature and feed concentration*

After successfully performing the initial percrystallization tests, the process was documented over a range of concentrations and temperatures, the results of which can be seen in Fig. 10. The experiments were performed from left to right, when viewing the graph, at feed temperatures of 50, 55 and 60°C. At each of the temperatures, the initial concentration of feed solution was varied to 0, 3.5, 10 and 17.5% (w/w). The range of fluxes measured at 50 °C seem consistently higher than those obtained at higher temperatures. It is important to note that, compared to other temperature driven membrane processes (e.g., membrane distillation), where only temperature-induced evaporation governs the flux, flux in percrystallization is determined by the rate of water permeation through the membrane and evaporation taking place from the surface. At high temperatures, the rate of water evaporation is high and rate of permeation through the membrane may become the flux-controlling parameter. Therefore, the flux does not necessarily increase with temperature. The low flux observed at high temperatures can be associated with possible blockage of some of the membrane pores due to precipitation of the salt inside the pores, which reduces the net permeation of liquid through the membrane.

It is observed that the water flux of the system at any temperature decreases with increase in initial salt concentration of feed solution. The observed decrease is higher at high operating temperature which is possibly due to the insufficient removal of water vapor from the system at high temperatures as was evident from more fog formation at the transparent surface of the flask at high temperature. Insufficient vapor removal suppresses the further evaporation of water from the surface which may have contributed to the observed low flux. However, it is worth mentioning that independent of the obtained value of flux at any condition, the process worked continuously over experimental period and produced continuous salts crystals from the solution. Low water flux at high temperatures also resulted into the corresponding low salt production rate as shown in the secondary axis of Fig. 10.

As MP3 membrane shows cracks on its surface, the stability of the membrane structure was validated by performing percrystallization test using 17.5% NaCl solution for 5 cycles – each cycle lasting for one hour. The hypothesis was that the deterioration of the structure should yield higher water flux as removal of coating layer will expose hydrophilic surface to the water. The membrane pores were flushed with the pure water between the tests and the flux was monitored over time for each of the tests. It was observed that the membrane showed consistent performance in terms of water flux (Fig. 11) during all the tests which demonstrated the stability of the porous structure during the operation.

It was observed during the series of experiments that the accumulation and release of salt crystals from the membrane surface is dependent upon the operative condition applied during the process. The cumulation and release behavior of the crystals at the membrane surface is divided into 3 main groups: shell formation, flake ejection and powder ejection as shown in Fig. 12. Shell formation tends to occur at low temperatures and low NaCl concentration and is characterized by continuous accumulation of the salt crystals at the membrane surface. Low temperature decreases the rate of evaporation, which favors crystal growth more than nucleation and the growing crystals also combine to form the crystal shell. The shell formation is considered unfavorable as it tends to slow down the percrystallization process and the process can stop eventually, due to the blockage of membrane pores.

At the other end of the spectrum, powder ejection is observed. This occurs at high NaCl concentration and high temperatures. High temperatures favor the rate of evaporation where the liquid-vapor transition is more rapid. The more rapid the crystallization occurs; the less time is available for crystal growth leading to the formation of relatively small crystals which are more easily ejected from the membrane surface. High temperature also helps in drying the formed crystals which reduces their adhesion with each other. The powder ejection is considered the most favorable to ensure the process stability and continuous operation.

Flake ejection is an intermediate mode as it shares characteristics of both shell formation and powder ejection and is observed in between the two extremes of temperature and concentration. Crystal growth is significant enough that shell formation occurs, however, the combined effect of applied vacuum and liquid-vapor transition dislodge flakes of the shell. This mode is still unfavorable, compared to powder ejection, as shell formation still occurs and over time this may hamper the process. Though our preliminary investigations indicate stable process operation at relatively high temperature and high solution concentrations, the effect of membrane surface properties (surface roughness, degree of hydrophobicity), degree of vacuum and nature of crystalline product are also expected to significantly impact the process stability by affecting

the release mechanism of crystals from the membrane surface.

3.9. Evaluation of percrystallization

Most of the fluxes from Fig. 10 are within the range of $9.43 \pm 2.02 \frac{kg}{m^2 hr}$, which can be used as a comparison to other membrane based ZLD desalination/wastewater treatments. The fluxes obtained in this study are comparable to those observed in direct contact membrane distillation (Alkhudhiri et al., 2012; Eykens et al., 2017) where for the experiments with feed temperatures from 50 °C to 60 °C, fluxes range from 11.6 to $20.2 \frac{kg}{m^2 hr}$ when pure water is used (J. Phattaranawik et al., 2003; J. Phattaranawik et al., 2003). However, the flux becomes comparable to that obtained in the current study when saline solutions are (Gryta, 2009; He et al., 2008; Warsinger et al., 2015). It should also be noted that the current study was performed under unoptimized conditions, which leaves margin of improvement in the flux. The fluxes obtained in this study are greater or comparable with most of those reported for direct concentration of minerals with forward osmosis (Ali et al., 2020) ($4.6 \frac{L}{m^2 hr}$ (Xue et al., 2015), $12 - 22.5 \frac{L}{m^2 hr}$ (Volpin et al., 2018), $8.5 - 4.2 \frac{L}{m^2 hr}$ (Hau et al., 2014) and $5.5 - 2.5 \frac{L}{m^2 hr}$ (Ali et al., 2020; Nguyen et al., 2013)). Moreover, percrystallization has the advantage that crystals and distilled water are separated in a single step without the need of filtration and drying.

The fluxes obtained in this study are higher than those reported for capillary percrystallization—percrystallization without vacuum— (2.1 $kg/m^2.h$ (Zhang et al., 2021) and 0.02 $L/m^2.h$ (Ji et al., 2022)). The increased flux for vacuum-assisted percrystallization compared to the capillary percrystallization is expected since the rate of evaporation is considered the slowest process, and this is greatly accelerated by applying a vacuum. However, the flux in our study is significantly lower than the studies on vacuum percrystallization reported in literature: $25.2 - 29 \frac{L}{m^2 hr}$ at 50 °C to 60 °C (R.S.K. Madsen et al., 2018), $33 \frac{L}{m^2 hr}$ (R.S. K. Madsen et al., 2018) and $20.1 \frac{L}{m^2 hr}$ (Motuzas et al., 2018) with the latter two at 37 °C. This can be attributed to the different degrees of applied vacuum which significantly affects the rate of permeation and evaporation. Moltedo et al. reported 30 mbar (Moltedo et al., 2022) and Madsen et al. reported 18, 22 and 26 mbar applied vacuum (R.S.K. Madsen et al., 2018) whereas this study uses 80 mbar.

We also investigated the effect of applied vacuum on flux for MP3 membrane operating at 50°C and the results have been shown in Fig. 13. It is evident from the figure that the obtained flux start approaching the values reported in the literature cited in the above paragraph when the degree of applied vacuum approaches to the values reported in those studies. However, it should be noted that the flux under any applied degree of vacuum will also depend upon the other membrane properties such as overall porosity and thermal conductivity of the membrane which determine the rate of water transport through the membrane and conductive heat transported from the fluid present inside the membrane to its surface. The low degree of vacuum becomes significant when upscaling the process. Low applied vacuum is easy to implement at large scale systems and can potentially be important to reduce electric energy consumption of the process as mentioned in our previous work (Simoni et al., 2021).

4. Conclusions

Commercial Si-C and PP hollow fiber membranes were studied to achieve zero liquid discharge in desalination through continuous vacuum percrystallization. It was observed that the permeation-controlling membrane parameters namely membrane thickness, porosity, and liquid entry pressure (determined by the surface hydrophobicity and pore size) were crucial to successfully operate the process. Thus, the membranes with very high permeability or liquid entry pressure greater than 1 bar were not suitable for the process and only the membranes with the permeation rate comparable to the evaporation rate under the applied vacuum worked well. By using the suitable membranes, dry salt crystals were obtained independent of the solution concentration or temperature conditions investigated, demonstrating the suitability of the developed membranes to achieve zero liquid discharge. Thus, the study brings percrystallization process for water and resource recovery from liquid streams one step closer to the commercial readiness. There is also preliminary indication that the process can potentially be used to tune the shape of the obtained crystals, however, further research is required to explore this aspect in more details. The developed membranes can also be interesting candidate to achieve the crystalline products from food, pharmaceutical and industrial wastewater streams. Fig. A2

CRediT authorship contribution statement

Morten Haugaard Nielsen: Methodology, Conceptualization, Investigation, Writing – original draft. **Cejna Quist-Jensen:** Resources, Writing – review & editing, Supervision. **Aamer Ali:** Conceptualization, Methodology, Writing – review & editing, Supervision.

Declaration of Competing Interest

The authors declare that they have no known competing financial interests or personal relationships that could have appeared to influence the work reported in this paper.

Data availability

No data was used for the research described in the article.

Acknowledgements

We are thankful to Haris Kadrispahic, research and development manager / head of innovation at LiqTech, who supplied the LiqTech silicon carbide membranes.

Appendix

X-ray diffraction analysis

Pulverized MP0 and MP1 membrane samples are analyzed via X-ray diffraction and the resulting diffractograms are displayed in Fig. A3. Both diffractograms share the same peaks sharp high amplitude peaks which confirm the crystalline structure of the membrane. The sharp peaks are located at 34.01, 35.6, 38.10, 41.40, 43.31, 45.25, 54.57, 59.89, 65.56, 71.73, 73.38, 75.47 and 78.35, the majority of these peaks overlap with those reported in literature and these demonstrate characteristics of hexagonal α Si-C crystalline structure (6H,α-SiC) (Kim et al., 2017; Ortiz et al., 2001). X-ray diffraction demonstrates that the coating of particles on the surface of an arbitrary modified membrane is insignificant when the bulk material is characterized as no broad amorphous peak is observed around ~24° as observed by X-ray diffraction of Silica particles synthesized by a modified Stöber method.

References

Alem, A., Sarpoolaky, H., Keshmiri, M., 2009a. Sol-gel preparation of titania multilayer membrane for photocatalytic applications. Ceram Int. 35 (5), 1837–1843. https://doi.org/10.1016/j.ceramint.2008.10.034. Jul.

Alem, A., Sarpoolaky, H., Keshmiri, M., 2009b. Titania ultrafiltration membrane: preparation, characterization and photocatalytic activity. J. Eur. Ceram Soc. 29 (4), 629–635. https://doi.org/10.1016/j.jeurceramsoc.2008.07.003. Mar.

Ali, A., et al., 2020. A review of membrane crystallization, forward osmosis and membrane capacitive deionization for liquid mining. Resour. Conserv. Recycl. 168, 2021. https://doi.org/10.1016/j.resconrec.2020.105273. August.

Ali, S.H., et al., 2017. Mineral supply for sustainable development requires resource governance. Nature 543 (7645), 367–372. https://doi.org/10.1038/nature21359.

Al-Karaghouli, A., Kazmerski, L.L., 2013. Energy consumption and water production cost of conventional and renewable-energy-powered desalination processes. Renew. Sustain. Energy Rev. 24, 343–356. https://doi.org/10.1016/j.rser.2012.12.064.

Alkhudhiri, A., Darwish, N., Hilal, N., 2012. Membrane distillation: a comprehensive review. Desalination 287, 2–18. https://doi.org/10.1016/j.desal.2011.08.027. Nov. 15.

Al-Kindi, I., Babadagli, T., 2021. Revisiting Kelvin equation and Peng–Robinson equation of state for accurate modeling of hydrocarbon phase behavior in nano capillaries. Sci. Rep. 11 (1) https://doi.org/10.1038/s41598-021-86075-8. Dec.

A. Beganskienė, V. Sirutkaitis, M. Kurtinaitienė, R. Juškėnas, and A. Kareiva, "FTIR, TEM and NMR Iinvestigations of Stöber Silica Nanoparticles," 2004.

Bhattacharjee, S., 2016. DLS and zeta potential - What they are and what they are not? J. Controlled Release 235, 337–351. https://doi.org/10.1016/j.jconrel.2016.06.017. Aug. 10,.

Chabanon, E., Mangin, D., Charcosset, C., 2016. Membranes and crystallization processes: state of the art and prospects. J. Memb. Sci. 509, 57–67. https://doi.org/10.1016/j.memsci.2016.02.051. Jul. 01.

Cortese, B., D'Amone, S., Manca, M., Viola, I., Cingolani, R., Gigli, G., 2008. Superhydrophobicity due to the hierarchical scale roughness of PDMS surfaces. Langmuir 24 (6), 2712–2718. https://doi.org/10.1021/la702764x. Mar.

Drioli, E., et al., 2013. Novel PVDF hollow fiber membranes for vacuum and direct contact membrane distillation applications. Sep. Purif. Technol. 115, 27–38. https://doi.org/10.1016/j.seppur.2013.04.040. Aug.

Drioli, E., di Profio, G., Curcio, E., 2012. Progress in membrane crystallization. Curr. Opin. Chem. Eng. 1 (2), 178–182. https://doi.org/10.1016/j.coche.2012.03.005.

M. Elimelech and W.A. Phillip, "The future of seawater desalination: energy, technology, and the environment," 2011. [Online]. Available: www.sciencemag.org.

Elshkaki, A., Graedel, T.E., Ciacci, L., Reck, B.K., 2018. Resource demand scenarios for the major metals. Environ. Sci. Technol. 52 (5), 2491–2497. https://doi.org/10.1021/acs.est.7b05154.

Eykens, L., de Sitter, K., Dotremont, C., Pinoy, L., van der Bruggen, B., 2017. Membrane synthesis for membrane distillation: a review. Sep. Purif. Technol. 182, 36–51. https://doi.org/10.1016/j.seppur.2017.03.035.

Franklin, et al., 1987. Wetting criteria for the applicability membrane distillation* of. J. Memb. Sci. 33, 315–328.

Gao, W., Rigout, M., Owens, H., 2016. Facile control of silica nanoparticles using a novel solvent varying method for the fabrication of artificial opal photonic crystals. J. Nanoparticle Res. 18 (12) https://doi.org/10.1007/s11051-016-3691-8. Dec.

Ghimire, P.P., Jaroniec, M., 2021. Renaissance of Stöber method for synthesis of colloidal particles: new developments and opportunities. J. Colloid Interface Sci. 584, 838–865. https://doi.org/10.1016/j.jcis.2020.10.014. Feb. 15.

Giang, H.N., et al., 2020. Fabrication of superhydrophobic surface using one-step chemical treatment. Surfaces and Interfaces 21. https://doi.org/10.1016/j.surfin.2020.100673. Dec.

Gryta, M., 2009. Calcium sulphate scaling in membrane distillation process. Chem. Papers 63 (2), 146–151. https://doi.org/10.2478/s11696-008-0095-y.

Gude, V.G., 2011. Energy consumption and recovery in reverse osmosis. Desalination Water Treat. 36 (1–3), 239–260. https://doi.org/10.5004/dwt.2011.2534.

Hau, N.T., Chen, S.S., Nguyen, N.C., Huang, K.Z., Ngo, H.H., Guo, W., 2014. Exploration of EDTA sodium salt as novel draw solution in forward osmosis process for dewatering of high nutrient sludge. J. Memb. Sci. 455, 305–311. https://doi.org/10.1016/j.memsci.2013.12.068. Apr.

He, F., Gilron, J., Lee, H., Song, L., Sirkar, K.K., 2008. Potential for scaling by sparingly soluble salts in crossflow DCMD.pdf. J. Memb. Sci. 311, 68–80.

Hinegardnrr, B.W.S, 2022. Needle-Shaped Crystals of Sodium Chloride. UTC [Online]. Available. https://pubs.acs.org/sharingguidelines.

Huertas, R.M., Fraga, M.C., Crespo, J.G., Pereira, V.J., 2017. Sol-gel membrane modification for enhanced photocatalytic activity. Sep. Purif. Technol. 180, 69–81. https://doi.org/10.1016/j.seppur.2017.02.047.

S. Hughes and J. Lau, "A technique for fast and accurate measurement of hand volumes using Archimedes' principle*," 2008. [Online]. Available: www.sartorius.com.

Ji, G., et al., 2022. A novel membrane-promoted crystallization process integrating water recovery and salt production for brine management. Chem. Eng. J. 430 https://doi.org/10.1016/j.cej.2021.133022. Feb.

Kim, S.C., Kim, Y.W., Song, I.H., 2017. Processing and properties of glass-bonded silicon carbide membrane supports. J. Eur. Ceram Soc. 37 (4), 1225–1232. https://doi.org/10.1016/j.jeurceramsoc.2016.11.019. Apr.

Li, J., et al., 2020. Superhydrophobic methylated silica sol for effective oil-water separation. Materials (Basel) 13 (4). https://doi.org/10.3390/ma13040842. Feb.

X. Ma et al., "Surfactant-assisted Fabrication of Alumina-doped Silica Nanofiltration Membranes with Enhanced Water Purification Performances," 2019.

Madsen, R.S.K., Motuzas, J., Julbe, A., Vaughan, J., Diniz, J.C., 2018a. Hydrometallurgy Novel membrane percrystallisation process for nickel sulphate production. Hydrometallurgy 185, 210–217. https://doi.org/10.1016/j.hydromet.2019.02.015. October2019.

Madsen, R.S.K., Motuzas, J., Julbe, A., Vaughan, J., Diniz da Costa, J.C., 2019. Novel membrane percrystallisation process for nickel sulphate production. Hydrometallurgy 185, 210–217. https://doi.org/10.1016/j.hydromet.2019.02.015. May.

Madsen, R.S.K., Motuzas, J., Vaughan, J., Julbe, A., Diniz da Costa, J.C., 2018b. Fine control of NaCl crystal size and particle size in percrystallisation by tuning the morphology of carbonised sucrose membranes. J. Memb. Sci. 567, 157–165. https://doi.org/10.1016/j.memsci.2018.09.003. Dec.

T. Matsoukas and E. Gulari, "Dynamics of growth of silica particles from ammonia-catalyzed hydrolysis of Tetra-ethyl-orthosilicate," 1988.

Mekonnen, M.M., Hoekstra, A.Y., 2016. Sustainability: four billion people facing severe water scarcity. Sci. Adv. 2 (2) https://doi.org/10.1126/sciadv.1500323. Feb.

Meybeck, M., 2003. Global analysis of river systems: from Earth system controls to Anthropocene syndromes. Philosophical Trans. Royal Society B: Biol. Sci. 358 (1440), 1935–1955. https://doi.org/10.1098/rstb.2003.1379. Dec. 29.

Moltedo, J.J., Schwarz, A., Gonzalez-Vogel, A., 2022. Evaluation of percrystallization coupled with electrodialysis for zero liquid discharge in the pulping industry. J Environ. Manag. 303 https://doi.org/10.1016/j.jenvman.2021.114104. Feb.

Motuzas, J., et al., 2018. Novel inorganic membrane for the percrystallization of mineral, food and pharmaceutical compounds. J. Memb. Sci. 550, 407–415. https://doi.org/10.1016/j.memsci.2017.12.077. Mar.

Nguyen, N.C., Chen, S.S., Yang, H.Y., Hau, N.T., 2013. Application of forward osmosis on dewatering of high nutrient sludge. Bioresour. Technol. 132, 224–229. https://doi.org/10.1016/j.biortech.2013.01.028.

Oren, Y., et al., 2010. Pilot studies on high recovery BWRO-EDR for near zero liquid discharge approach. Desalination 261 (3), 321–330. https://doi.org/10.1016/j.desal.2010.06.010.

A.L. Ortiz, F. Sanchez-Bajo, F.L. Cumbrera, and F. Guiberteau, "X-ray powder diffraction analysis of a silicon carbide-based ceramic," 2001. [Online]. Available: www.elsevier.comrlocatermatlet.

Panagopoulos, A., Haralambous, K.J., 2020a. Minimal liquid discharge (MLD) and zero liquid discharge (ZLD) strategies for wastewater management and resource recovery-analysis, challenges and prospects. J. Environ. Chem. Eng. 8 (5) https://doi.org/10.1016/j.jece.2020.104418. Oct.

Panagopoulos, A., Haralambous, K.J., 2020b. Environmental impacts of desalination and brine treatment - challenges and mitigation measures. Mar. Pollut. Bull. 161 https://doi.org/10.1016/j.marpolbul.2020.111773. Dec. 01.

S.K. Park, K. do Kim, and H.T. Kim, "Preparation of silica nanoparticles: determination of the optimal synthesis conditions for small and uniform particles," 2002. [Online]. Available: www.elsevier.com/locate/colsurfa.

Peter, G., 1993. World'S Fresh Water Resources. Water In Crisis - A Guide to the World`s Fresh Water Resources.

Phattaranawik, J., Jiraratananon, R., Fane, A.G., 2003a. Effect of pore size distribution and air flux on mass transport in direct contact membrane distillation. J. Memb. Sci. 215 (1–2), 75–85. https://doi.org/10.1016/S0376-7388(02)00603-8. Apr.

J. Phattaranawik, R. Jiraratananon, and A.G. Fane, "Heat transport and membrane distillation coefficients in direct contact membrane distillation," 2003.

V. Purcar, O. Cinteza, M. Ghiurea, A. Balan, S. Caprarescu, and D. Donescu, "Influence of hydrophobic characteristic of organo-modified precursor on wettability of silica film," 2014.

Schwarzenbach, R.P., Egli, T., Hofstetter, T.B., von Gunten, U., Wehrli, B., 2010. Global water pollution and human health. Annu. Rev. Environ. Resour. 35, 109–136. https://doi.org/10.1146/annurev-environ-100809-125342. Nov.

Simoni, G., Kirkebæk, B.S., Quist-Jensen, C.A., Christensen, M.L., Ali, A., 2021. A comparison of vacuum and direct contact membrane distillation for phosphorus and ammonia recovery from wastewater. J. Water Process Eng. 44 https://doi.org/10.1016/j.jwpe.2021.102350. Dec.

R. Skov and K. Madsen, "Novel percrystallisation process by inorganic carbon membranes," 1968.

W. Stober, A. Fink, and D.Ernst Bohn, "Controlled growth of monodisperse silica spheres in the micron size range 1," 1968.

Tadanaga, K., Morita, K., Mori, K., Tatsumisago, M., 2013. Synthesis of monodispersed silica nanoparticles with high concentration by the Stöber process. J. Solgel Sci. Technol. 68 (2), 341–345. https://doi.org/10.1007/s10971-013-3175-6. Nov.

Tauber, H., Kleiner, I.S., 1932a. A Convenient Method for the Crystallization of Sugars and Other Organic Substances, 6. Crytallization of substances, pp. 2392–2393.

Tauber, H., Kleiner, I.S., 1932b. Needle-shaped crystals of sodium chloride obtained by percrystallization. J. Am. Chem. Soc. 54 (6), 2392–2393 [Online]. Available. https://pubs.acs.org/sharingguidelines.

Tong, T., Elimelech, M., 2016. The global rise of zero liquid discharge for wastewater management: drivers, technologies, and future directions. Environ. Sci. Technol. 50 (13), 6846–6855. https://doi.org/10.1021/acs.est.6b01000. Jul. 05.

van Enckevort, W.J.P., Los, J.H., 2013. On the creeping of saturated salt solutions. Cryst. Growth Des. 13 (5), 1838–1848. https://doi.org/10.1021/cg301429g. May.

Vergili, I., Kaya, Y., Sen, U., Gönder, Z.B., Aydiner, C., 2012. Techno-economic analysis of textile dye bath wastewater treatment by integrated membrane processes under the zero liquid discharge approach. Resour. Conserv. Recycl. 58, 25–35. https://doi.org/10.1016/j.resconrec.2011.10.005. Jan.

Volpin, F., Fons, E., Chekli, L., Kim, J.E., Jang, A., Shon, H.K., 2018. Hybrid forward osmosis-reverse osmosis for wastewater reuse and seawater desalination: understanding the optimal feed solution to minimise fouling. Process Safety and Environ. Protection 117, 523–532. https://doi.org/10.1016/j.psep.2018.05.006. Jul.

Vörösmarty, C.J., et al., 2010. Global threats to human water security and river biodiversity. Nature 467 (7315), 555–561. https://doi.org/10.1038/nature09440. Sep.

Warsinger, D.M., Swaminathan, J., Guillen-Burrieza, E., Arafat, H.A., Lienhard V, J.H., 2015. Scaling and fouling in membrane distillation for desalination applications: a review. Desalination 356, 294–313. https://doi.org/10.1016/j.desal.2014.06.031.

G. Wolansky and A. Marmur, "Apparent contact angles on rough surfaces: the Wenzel equation revisited," 1999. [Online]. Available: www.elsevier.nl/locate/colsurfa.

Xue, W., Tobino, T., Nakajima, F., Yamamoto, K., 2015. Seawater-driven forward osmosis for enriching nitrogen and phosphorous in treated municipal wastewater: effect of membrane properties and feed solution chemistry. Water Res. 69, 120–130. https://doi.org/10.1016/j.watres.2014.11.007. Feb.

T. Yamamoto, K. Haraga, and M. Tashiro, "Identification of crystals protruding from surface of Na20.3SiO2 glass," 1973.
Yang, H., et al., 2010. Facile preparation of super-hydrophobic and super-oleophilic silica film on stainless steel mesh via sol-gel process. Appl. Surf. Sci. 256 (13), 4095–4102. https://doi.org/10.1016/j.apsusc.2010.01.090. Apr.
Yaqub, Muhammad, Lee, W., 2019. Zero-liquid discharge (ZLD) technology for resource recovery from wastewater: a review. Sci. Total Environ. 681, 551–563. https://doi.org/10.1016/j.scitotenv.2019.05.062. Sep. 01.
Zhang, C., et al., 2021. Designing a next generation solar crystallizer for real seawater brine treatment with zero liquid discharge. Nat. Commun. 12 (1) https://doi.org/10.1038/s41467-021-21124-4. Dec.
Y. Zhang, (2021) "The effect of surface roughness parameters on contact and wettability of solid surfaces." [Online]. Available: https://lib.dr.iastate.edu/rtd/15934.